PREDICTION OF LOCAL PENETRATION/DAMAGE AND GLOBAL DYNAMIC SYSTEM RESPONSE FOR LETHALITY/SURVIVABILITY: A MULTI-TIME SCALE APPROACH

Y. Miller*

Department of Civil and Mechanical Engineering
United States Military Academy, West Point

X. Zhou, D. Sha, and K. K. Tamma

Department of Mechanical Engineering, University of Minnesota
Army High Performance Computing Research Center, Minneapolis, MN 55455

ABSTRACT

The Future Combat Systems (FCS) will transform the Army into a faster, more agile force with more lethal and more survivable capabilities. The FCS requires computational technologies that can simulate and assess lethality and survivability of the combat systems under real battlefield situations involving the global structural dynamics at system level, and highly localized contact-impact, damage, failure, penetration, and fragmentation. In order to integrate the aforementioned capabilities into a standalone computational code, a computational framework taking into consideration different mechanics descriptions and formulations, different physical events such as structural dynamics, contact-impact, damage, failure, penetration, and fragmentation need to be carefully addressed. In this regard, different computational formulations in space such as finite element methods and meshless methods, and in time such as implicit algorithms, explicit algorithms, and the like need to be seamlessly integrated. Existing technologies focus on an isolated physical event or a limited coupled physical event. A computational framework that can integrate the aforementioned multi-physical events for combat systems commonly encountered in real battlefield situations does not exist to-date. We address the above issues with applications to engineering problems, and the present approach compares well with experimental results.

1. INTRODUCTION

Hydrocodes are important tools for survivability and lethality of armor/anti-armor applications [Schraml et al., 2002]. The existing hydrocodes mostly utilize fracture mechanics based failure models (the failure of the material is determined by the maximum accumulated plastic strain) [Zukas, 2004]. In contrast to the fracture mechanics based failure models, which focus on when the material fails, the continuum damage mechanics based failure models (the failure of the material is determined by the evolution of an internal variable that measures the micro-defect density) can further provide an in-depth understanding of the physical mechanisms of how the material fails [Krajcinovic, 2000]. Furthermore, since Lemaitre introduced an approach to incorporate fracture mechanics based failure model into the continuum damage mechanics based isotropic damage failure models [Lemaitre, 1985a, Lemaitre, 1985b], the Lemaitre damage model has been successfully applied for the quasi-static failure of steel [Celentano et al., 2004] and high-velocity penetration [Børvik et al., 2001]. The present study aims to extend the Lemaitre damage model to the hydrodynamic type of constitutive model for high velocity penetration problems.

With the objective towards the development of a computational framework that can simulate the integrated multi-physics and multi-time scale battlefield events, the development of highly efficient and scalable multi-time scale and adaptive semi-implicit/explicit hybrid dynamic computational is the key for predicting both the long term global dynamic response of structural systems such as the entire transient response of the combat system and structural configuration, in conjunction with effects imparted due to localized short term dynamic damage due to threats such as penetration. Quite often, a representative section of the vehicle component is mostly considered (for example a small armor plate section) for the simulation in survivability/lethality designs. Increasing model fidelity requires high mesh resolutions. Longer simulation times are additionally needed to assess post dynamic simulations at the system level due to localized contact-impact-penetration-damage events. Computational requirements grow dramatically as the size

Report Documentation Page

Form Approved
OMB No. 0704-0188

Public reporting burden for the collection of information is estimated to average 1 hour per response, including the time for reviewing instructions, searching existing data sources, gathering and maintaining the data needed, and completing and reviewing the collection of information. Send comments regarding this burden estimate or any other aspect of this collection of information, including suggestions for reducing this burden, to Washington Headquarters Services, Directorate for Information Operations and Reports, 1215 Jefferson Davis Highway, Suite 1204, Arlington VA 22202-4302. Respondents should be aware that notwithstanding any other provision of law, no person shall be subject to a penalty for failing to comply with a collection of information if it does not display a currently valid OMB control number.

1. REPORT DATE	2. REPORT TYPE	3. DATES COVERED
01 NOV 2006	**N/A**	**-**

4. TITLE AND SUBTITLE	5a. CONTRACT NUMBER
Prediction Of Local Penetration/Damage And Global Dynamic System Response For Lethality/Survivability: A Multi-Time Scale Approach	5b. GRANT NUMBER
	5c. PROGRAM ELEMENT NUMBER
6. AUTHOR(S)	5d. PROJECT NUMBER
	5e. TASK NUMBER
	5f. WORK UNIT NUMBER
7. PERFORMING ORGANIZATION NAME(S) AND ADDRESS(ES) **Department of Civil and Mechanical Engineering United States Military Academy, West Point**	8. PERFORMING ORGANIZATION REPORT NUMBER
9. SPONSORING/MONITORING AGENCY NAME(S) AND ADDRESS(ES)	10. SPONSOR/MONITOR'S ACRONYM(S)
	11. SPONSOR/MONITOR'S REPORT NUMBER(S)

12. DISTRIBUTION/AVAILABILITY STATEMENT
Approved for public release, distribution unlimited

13. SUPPLEMENTARY NOTES
See also ADM002075., The original document contains color images.

14. ABSTRACT

15. SUBJECT TERMS

16. SECURITY CLASSIFICATION OF:			17. LIMITATION OF ABSTRACT	18. NUMBER OF PAGES	19a. NAME OF RESPONSIBLE PERSON
a. REPORT	b. ABSTRACT	c. THIS PAGE			
unclassified	**unclassified**	**unclassified**	**UU**	**8**	

Standard Form 298 (Rev. 8-98)
Prescribed by ANSI Std Z39-18

and complexity of the computational models increase. As the element size is decreased to capture the finer details such as large deformations in geometry and for overall response, the time step also significantly decreases. This is especially cumbersome and also impractical for large-scale simulations such as an entire Army vehicle system to be completed in reasonable time. Using traditional explicit and implicit finite element codes, the coupling of standalone explicit and implicit codes is not feasible and/or practical due to: 1) approximation errors in transferring results from one code to the other, and 2) impractical to do data transfer if damage, penetration and fragmentation are involved with flying debris. Towards this end, the present efforts circumvent several existing drawbacks via new computational methods and algorithms and include the total integration and fusion of various computational technologies. Therefore, an approach of adaptive multi-scale semi-implicit/explicit hybrid formulations and computational algorithms would capitalize upon both the advantages of implicit and explicit time integration algorithms to avoid the existing drawbacks and is desirable for the simulations of numerous applications involving lethality and survivability. Such a hybrid approach is not feasible within the standard framework of linear multi-step (LMS) methods that exist in most Lagrangian codes [Zhou and Tamma, 2004]. The approach for developing hybrid and adaptive multi-scale computational algorithms is based on the recent and highly successful developments of robust element based smart-switch algorithms in time which smartly switch on/off the necessary algorithms on an element basis for the given simulation model (between a semi-implicit formulation which do not require any nonlinear iterations [Zhou et al., 2005] and a explicit time formulations [Sha et al., 1996], both of which have been derived from a novel theory on the time dimension). The automated built-in switch is based on the element physical and geometrical measures, and on the state of the damage variables; as a consequence, if the time steps for explicit elements in the numerical mesh become prohibitively small due to severe large deformations and distortions, only the corresponding elements are switched to semi-implicit formulations with a much larger time step. Time adaptive features are embedded into the framework to provide optimal time steps for assessing both short/long term dynamic simulations. Since the total simulation framework of semi-implicit time formulations is readily integrated to the naturally scalable explicit formulations while the load balancing is performed appropriately, the overall HPC simulations can readily handle the multiple time scale applications.

The presentation of this exposition is outlined as the follows. First the dynamic equilibrium equation including frictional contact boundary conditions in Eulerian form is formulated. Then the deviatoric portion of the hydrodynamic constitutive equation incorporating the elasto-visco-thermo-plastic-damage is formulated. And, the hydrostatic portion of the hydrodynamic constitutive equation utilizing the equation of state and internal energy equation is then discussed. The time integration procedure is described. Finally, numerical validation are performed to demonstrate the applicability and robustness of the present computational framework and formulation.

2. EQUATION OF MOTION

Let the open set $\Omega_t \subset \Re^3$ be the domain of interest of the configuration at time t, with the boundary $\partial\Omega_t = \Gamma_t^f \cup \Gamma_t^d$, $\Gamma_t^f \cap \Gamma_t^d = \emptyset$, and the closure $\overline{\Omega}_t = \Omega_t \cup \partial\Omega_t$. For finite strain dynamic problems, the dynamic equilibrium equation of the configuration at time t in the Eulerian form with Cauchy stress is described by

$$\frac{\partial(\rho_t \boldsymbol{v}_t)}{\partial t} + \rho_t \eta \boldsymbol{v}_t - \nabla \cdot \boldsymbol{\sigma}_t = \boldsymbol{b}_t \quad in \quad \Omega_t \quad (1)$$

$$\boldsymbol{\sigma}_t \boldsymbol{n} = f \quad on \quad \Gamma_t^f \quad (2)$$

$$\boldsymbol{x}_t = \boldsymbol{x}^d \quad on \quad \Gamma_t^d \quad (3)$$

where ρ_t is the material density of the configuration at time t, $\boldsymbol{v}_t$ is the material particle velocity at time t, $\boldsymbol{\sigma}_t$ is the Cauchy stress of the configuration at time t, η is the viscous damping ratio in the sense of Rayleigh damping, $\boldsymbol{b}_t$ is the body force, $\boldsymbol{n}$ is the boundary surface outward unit vector, $\boldsymbol{x}_t$ is material particle coordinate, Γ_t^f is the boundary subject to traction boundary condition, Γ_t^d is the boundary subject to prescribed displacement boundary condition.

Let $\boldsymbol{\sigma}_n = \boldsymbol{\sigma}\boldsymbol{n} = \{\sigma_{n_k}\} = -\{n_i \sigma_{ij} n_j n_k\} \in \Re^3$ be the normal stress on the contact surface, $\boldsymbol{n}$ be the normal direction vector on the contact surface, $\boldsymbol{g} \in \Re^3$ be the relative gap vector between point pairs on the contact surfaces. Let $\boldsymbol{g}_n$ and $\boldsymbol{g}_\tau$ be the normal and tangential directions of the gap vector $\boldsymbol{g}$, then $\boldsymbol{g} = \boldsymbol{g}_n + \boldsymbol{g}_\tau$ and $\boldsymbol{g}_n \cdot \boldsymbol{g}_\tau = 0$. And, the impenetrable constraint in the normal direction on the contact surfaces is given as the following Kuhn-Tucker complementarity conditions, $(\boldsymbol{\tau}_n, \boldsymbol{g}_n - \lambda_n^c \boldsymbol{n})_{\Gamma_c(t)} = 0$, $\lambda_n^c \geq 0$, $\psi_n(\boldsymbol{\sigma}_n) = \boldsymbol{\sigma} \cdot \boldsymbol{n} \geq 0$, $\lambda_n^c \psi_n(\boldsymbol{\sigma}_n) = 0$, $\forall\ \boldsymbol{\tau}_n \in \psi_n(\boldsymbol{\tau}_n) \geq 0$, where $\lambda_n^c \geq 0$ represents the impenetrability condition on the contact surface, and $(\bullet, \bullet)_\Gamma = \int_\Gamma \bullet : \bullet ds$ represents the inner-product.

Let $\boldsymbol{\mathcal{R}} = \{\boldsymbol{\mathcal{V}} \mid \boldsymbol{\mathcal{V}} \in \Re^3 \times [0, \infty)\}$, then a *yield function* of the frictional stress vector in the tangential direction on the contact surface can be defined by $\psi_\tau(\boldsymbol{\sigma}_\tau) = \mu^c \mid \boldsymbol{\sigma}_n \mid - \mid \boldsymbol{\sigma}_\tau \mid \geq 0$ on $\Gamma_c \times [0, \infty)$, where $\boldsymbol{\sigma}_\tau = \{\sigma_{t_k}\} = -\{n_i \sigma_{ik} - n_i \sigma_{kj} n_j n_k\} \in \Re^3$ is the tangential stress vector on the contact surface, and $\mu^c \in \Re$ is the Coulomb frictional coefficient.

Let $\dot{\boldsymbol{g}}_\tau \in \Re^3$ be the the relative tangential velocity of the point pairs on the contact surfaces, the classical Coulomb friction law thus is represented by $(\boldsymbol{\tau}_\tau - \boldsymbol{\sigma}_\tau, \dot{\boldsymbol{g}}_\tau) \leq 0$, $\boldsymbol{\sigma}_\tau \in \psi_\tau(\boldsymbol{\sigma}_\tau) \geq 0$, $\forall\ \boldsymbol{\tau}_\tau \in \psi_\tau(\boldsymbol{\tau}_\tau) \geq 0$. The corresponding weak form employing the Lagrangian multiplier is given as $(\boldsymbol{\tau}_\tau, \dot{\boldsymbol{g}}_\tau - \lambda_\tau^c \nabla_{\sigma_\tau}\psi_\tau(\boldsymbol{\sigma}_\tau))_{\Gamma_c(t)} = 0$, $\psi_\tau(\boldsymbol{\sigma}_\tau) \geq 0$, $\lambda_\tau^c \geq 0$, $\lambda_\tau^c \psi_\tau(\boldsymbol{\sigma}_\tau) = 0$, $\forall\ \boldsymbol{\tau}_\tau \in \psi_\tau(\boldsymbol{\tau}_\tau) \geq 0$, where $\nabla_{\sigma_\tau}\psi_\tau(\boldsymbol{\sigma}_\tau) = \frac{\partial \psi_\tau(\boldsymbol{\sigma}_\tau)}{\partial \boldsymbol{\sigma}_\tau}$.

Define the following set of virtual displacement field as, $[H_0^1(\Omega_t)]^3 := \{\boldsymbol{w} \mid \boldsymbol{w} \in [H^1(\Omega)]^3,\ \boldsymbol{w} = \boldsymbol{0} \text{ on } \Gamma^d\}$, and the set of virtual velocity field as, $[H_v^1(\Omega_t)]^3 := \{\boldsymbol{v} \mid \boldsymbol{v} \in [H^1(\Omega)]^3,\ \boldsymbol{v} = \dot{\boldsymbol{x}}_t^d \text{ on } \Gamma^d\}$, where $H^1(\Omega)$ is the first order differentiable Hilbert space. The Eulerian weak form of the dynamic equilibrium equation subjected to the contact boundary condition is given as the following.

$$
\begin{aligned}
&(\boldsymbol{w}, \tfrac{\partial(\rho \boldsymbol{v})}{\partial t} + \rho \eta \boldsymbol{v})_{\Omega_t} + (\boldsymbol{\mathcal{D}}(\boldsymbol{w}), \boldsymbol{\sigma})_{\Omega_t} \\
= \quad &(\boldsymbol{w}, \boldsymbol{b})_{\Omega_t} + (\boldsymbol{w}, \boldsymbol{f})_{\Gamma_f(t)} + (\delta \boldsymbol{g}, \boldsymbol{\sigma}_n + \boldsymbol{\sigma}_\tau)_{\Gamma_c(t)} \quad (4) \\
&(\boldsymbol{\tau}_n, \boldsymbol{g}_n - \lambda_n^c \boldsymbol{n})_{\Gamma_c(t)} = 0 \quad (5) \\
&(\boldsymbol{\tau}_\tau, \dot{\boldsymbol{g}}_\tau - \lambda_\tau^c \nabla_{\sigma_\tau}\psi_\tau(\boldsymbol{\sigma}_\tau))_{\Gamma_c(t)} = 0 \quad (6)
\end{aligned}
$$

and subject to the constraints $\lambda_n^c \geq 0$, $\psi_n(\boldsymbol{\sigma}_n) = \boldsymbol{\sigma}_n \cdot \boldsymbol{n} \geq 0$, $\lambda_n^c \psi_n(\boldsymbol{\sigma}_n) = 0$, on $\Gamma_c(t)$, and $\psi_\tau(\boldsymbol{\sigma}_\tau) \geq 0$, $\lambda_\tau^c \geq 0$, $\lambda_\tau^c \psi_\tau(\boldsymbol{\sigma}_\tau) = 0$, on $\Gamma_c(t)$.

In the matrix form, the equation of motion can be written as,

$$
\begin{aligned}
\mathbf{M}\ddot{\mathbf{u}} + \mathbf{C}\dot{\mathbf{u}} + \mathbf{K}\mathbf{u} &= \mathbf{f}(t) + \mathbf{G}^\top \mathbf{s}_T + \mathbf{G}^\top \mathbf{N}\phi \quad (7) \\
\lambda &= \mathbf{N}^\top \mathbf{G}(\mathbf{x} + \mathbf{u}) \geq 0 \quad (8) \\
\phi &\geq 0 \quad (9) \\
\lambda^\top \phi &= 0 \quad (10) \\
\dot{\mathbf{s}}_T &= -\frac{1}{\epsilon}(\dot{\mathbf{g}}_T + \mathbf{A}\dot{\lambda}_T) \quad (11) \\
\mu|\phi|_a - ||\mathbf{s}_T||_a &\geq 0 \quad (12)
\end{aligned}
$$

where $\mathbf{M}$ is the mass matrix, $\mathbf{C}$ is the damping matrix, $\mathbf{K}$ is the stiffness matrix, $\ddot{\mathbf{u}}$ is the acceleration, $\dot{\mathbf{u}}$ is the velocity, and $\mathbf{u}$ is the displacement, $\mathbf{f}$ is the external loading, $\mathbf{G}$ is the constraint matrix, $\mathbf{s}_T$ is the tangential contact force, $\mathbf{N}$ is the normal gap matrix, ϕ is the normal contact force magnitude, λ is the normal gap magnitude, $\mathbf{x}$ is the position vector, μ is the Coulomb coefficition of friction, $\mathbf{A}$ is the tangential gap matrix, and ϵ is an infinitesimal positive number.

3. CONSTITUTIVE EQUATION

Consider the isotropic damage hydrodynamic constitutive equation given by,

$$
\begin{cases}
\widetilde{\boldsymbol{\sigma}} = \dfrac{\boldsymbol{\sigma}}{1-\varphi} = \widetilde{\boldsymbol{\sigma}}_D + \widetilde{\boldsymbol{\sigma}}_H \\
\widetilde{\boldsymbol{\sigma}}_D^\nabla = 2G\boldsymbol{\mathcal{D}}_D^e \\
\widetilde{\boldsymbol{\sigma}}_H = -p(\rho, e)\boldsymbol{I}
\end{cases} \quad (13)
$$

where $\widetilde{\boldsymbol{\sigma}}$ is the effective stress tensor, $\boldsymbol{\sigma}$ is the Cauchy stress tensor, φ is the isotropic damage state variable, $\widetilde{\boldsymbol{\sigma}}_D$ is the deviatoric portion of the effective stress tensor, $\widetilde{\boldsymbol{\sigma}}_H$ is the hydrostatic portion of the effective stress tensor, G is the shear modulus, $\boldsymbol{\mathcal{D}}_D^e$ is the elastic part for the deviatoric portion of the velocity strain tensor, p is the hydrostatic pressure, ρ is the material density, e is the internal energy per unit mass, $\boldsymbol{I}$ is the rank two identity tensor, and the symbol $\bullet^\nabla$ denotes to either the Jaunamm, the Green-Naghdi, or Truesdell stress rate.

3.1 Damage Models for the Deviatoric Stress

From a practical perspective, the Lemaitre plastic-damage model [Lemaitre, 1996] is adapted for the deviatoric stress of the hydrodynamic constitutive equation. For the low- and high-velocity impact/penetration problems, when the amount of dissipative work done by the plasticity and damage in the system does not raise the temperature significantly, for example, a projectile impacting on a thin structure, the Lemaitre plastic-damage model should be applicable. However, when the amount of dissipative work gives rise to a rapid increase of temperature for the material, for example, in the case of hypervelocity penetration problems, a temperature dependent thermo-visco-plastic model such as the Johnson-Cook fracture model [Johnson and Cook, 1985] needs to be modified and incorporated into the Lemaitre plastic-damage model to account for the temperature and strain rate effect. The modified Johnson-Cook thermo-visco-plastic-damage model is described next.

The von Mises tensile flow stress of the Johnson-Cook model [Johnson and Cook, 1985] is given by,

$$
\sigma_{JC} = (A + B\varepsilon^n)(1 + C\ln(\frac{\dot{\varepsilon}}{\dot{\varepsilon}_0}))(1 - \tilde{T}^m) \quad (14)
$$

where A, B, C, n, and m are material constants, $\varepsilon_0 = 1.0s^{-1}$, $\tilde{T} = (T - T_{room})/(T_{melt} - T_{room})$, T_{room} is the room temperature, T_{melt} is the material melting temperature. And the fracture strain of the Johnson-Cook model [Johnson and Cook, 1985] is given by

$$
\varepsilon_F = (D_1 + D_2 e^{D_3 \frac{\sigma_H}{\sigma_{eq}}})(1 + D_4 \ln(\frac{\dot{\varepsilon}}{\dot{\varepsilon}_0}))(1 + D_5 \tilde{T}) \quad (15)
$$

for $\frac{\sigma_H}{\sigma_{eq}} < 1.5$, where D_1-D_5 are material constants. For $\frac{\sigma_H}{\sigma_{eq}} \geq 1.5$, the model becomes

$$
\varepsilon_F = (D_1 + D_2 e^{1.5 D_3})(1 + D_4 \ln(\frac{\dot{\varepsilon}}{\dot{\varepsilon}_0}))(1 + D_5 \tilde{T}) \quad (16)
$$

Let the thermo-visco-plastic-damage potential function be

$$
\begin{aligned}
&F_{tvpd}(\boldsymbol{\sigma}, R_{tvp}(\varepsilon), \mathcal{Q}^{-1}(\dot{\varepsilon}); Y, \varphi) \\
=&f_{tvp}(\boldsymbol{\sigma}, R_{tvp}(\varepsilon), \mathcal{Q}^{-1}(\dot{\varepsilon}); \varphi) + f_d(Y, \varphi)
\end{aligned} \quad (17)
$$

where

$$
\begin{aligned}
f_{tvp} &= \widetilde{\sigma}_{eq} - R_{tvp}(\varepsilon) - \mathcal{Q}^{-1}(\dot{\varepsilon}) \leq 0 && (18)\\
R_{tvp} &= (A + B\varepsilon^n)(1 - \tilde{T}^m) && (19)\\
\mathcal{Q}^{-1}(\dot{\varepsilon}) &= f_{rp} = CR_{tvp}\ln(\frac{\dot{\varepsilon}}{\dot{\varepsilon}_0}) && (20)\\
\mathcal{Q}(f_{rp}) &= \dot{\varepsilon} = \dot{\varepsilon}_0 e^{\frac{f_{rp}}{CR_{tvp}}} H(f_{rp}) && (21)
\end{aligned}
$$

Y is the energy release rate density, f_d is the damage potential, φ is the damage internal variable, and $H(\bullet)$ is the Heaviside function.

Thus, the Modified Johnson-Cook thermo-visco-plastic-damage model yields the constitutive equation in consistent form as

$$
\boldsymbol{\sigma}_D^{\nabla} = (1-\varphi)\left(\boldsymbol{\mathcal{C}} - \frac{\boldsymbol{\mathcal{C}} : \boldsymbol{n}^{tvpd} \otimes \boldsymbol{n}^{tvpd} : \boldsymbol{\mathcal{C}}}{\boldsymbol{n}^{tvpd} : \boldsymbol{\mathcal{C}} : \boldsymbol{n}^{tvpd} + H^{tvpd}}\right) : \boldsymbol{\mathcal{D}}_D \tag{22}
$$

where

$$
\begin{aligned}
H^{tvpd} &= h + C(h + \frac{\dot{\varepsilon}_0 R_{tvp}}{\dot{\varepsilon}\Delta t})\ln(\frac{\dot{\varepsilon}}{\dot{\varepsilon}_0}) \\
&\quad - \frac{H(\varepsilon - \varepsilon_D)\sigma_{eq}}{(1-\varphi)^2(\varepsilon_F - \varepsilon_D)} && (23)\\
h &= Bn\varepsilon^{n-1}(1 - \tilde{T}^m) && (24)\\
\boldsymbol{n}^{tvp} &= \frac{3\boldsymbol{\sigma}_D}{2\sigma_{eq}} && (25)
\end{aligned}
$$

Temperature for Adiabatic Condition
During the high strain rate deformation, the temperature of the material rises due to the dissipative plastic work. For the short duration of the material deformation under high strain rate, the thermal equilibrium of the material cannot be established. Therefore, the temperature raise can be computed by utilizing the adiabatic condition. And, the temperature equation is given as,

$$
\rho c\dot{T} = \eta_e \boldsymbol{\sigma} : (\boldsymbol{\mathcal{D}}_D - \boldsymbol{\mathcal{D}}_D^e) \tag{26}
$$

where ρ is the material density, c is the material heat capacity, and $\eta_e = 0.9$ is efficiency ratio [Bammann et al., 1993].

3.2 Equation of State for the Hydrostatic Pressure

The equation of state (EOS) along with the material internal energy equation governs the relation between the pressure and density implicitly, and serves as the constitutive equations which express the state that the material can achieve [Walsh and Christian, 1955]. The rate of internal energy per current unit mass is given as

$$
\dot{e} = \frac{1}{\rho}(\boldsymbol{\sigma}_D : \boldsymbol{\mathcal{D}} - p\ tr(\boldsymbol{\mathcal{D}})) \tag{27}
$$

where p is the hydrostatic pressure, and $tr(\boldsymbol{\mathcal{D}})$ is the trace of the velocity strain. And, the Mie-Grüneisen equation of state [Walsh et al., 1957] considered here is given by

$$
p(\rho, e) = (1 - \frac{1}{2}\gamma\mu)p_H + \gamma\rho e \tag{28}
$$

where $\mu = \eta - 1$, $\eta = \rho/\rho_0$, ρ_0 is the material density at the initial reference state, γ is the Grüneisen parameter, γ_0 is the Grüneisen parameter at the initial reference state, p_H is the Hugoniot pressure at the density ρ.

Let $\boldsymbol{\sigma}_D^{t+\Delta t}$ be the deviatoric Cauchy stress at time $t+\Delta t$ obtained from the deviatoric part of the hydrodynamic constitutive relation, a time integration algorithm for solving the hydrostatic pressure from the equation of state is given as the following.

Algorithm 1
For the time increment from t to $t+\Delta t$, the hydrostatic pressure can be integrated from following algorithm.

$$
p^{t+\Delta t} = \frac{A_{eos} + B_{eos}\tilde{e}^{t+\Delta t}\rho^{t+\Delta t}}{1 + 3B_{eos}\beta\Delta\mathcal{E}_H^{t+\Delta t}} \tag{29}
$$

where

$$
\begin{aligned}
A_{eos} &= (1 - \frac{1}{2}\gamma\mu)p_H && (30)\\
B_{eos} &= \gamma && (31)\\
\tilde{e}^{t+\Delta t} &= e^t + \frac{1}{\rho^{t+\Delta t}}\Big[(\alpha\boldsymbol{\sigma}_D^t + \beta\boldsymbol{\sigma}_D^{t+\Delta t}) : \Delta\boldsymbol{\mathcal{E}}^{t+\Delta t} \\
&\quad -3\alpha p^t \Delta\mathcal{E}_H^{t+\Delta t}\Big] && (32)\\
\Delta\boldsymbol{\mathcal{E}}^{t+\Delta t} &= \int_t^{t+\Delta t} \boldsymbol{\mathcal{D}} dt' && (33)\\
\Delta\mathcal{E}_H^{t+\Delta t} &= \int_t^{t+\Delta t} \mathcal{D}_H dt' && (34)\\
\mathcal{D}_H &= \frac{1}{3} trace(\boldsymbol{\mathcal{D}}) && (35)\\
\boldsymbol{\sigma}_D &= (1-\varphi)\widetilde{\boldsymbol{\sigma}}_D && (36)\\
\beta &= 1 - \alpha && (37)
\end{aligned}
$$

Artificial Viscosity
For numerical shock wave computation, the artificial viscosity is needed to stabilize the numerical oscillation [von Neumann and Richtmyer, 1950]. The classical artificial viscosity is adapted as the following.

$$
q = \begin{cases} \alpha_1\Delta x^2\rho\mathcal{D}_H^2 + \alpha_2\Delta x\rho\mathcal{D}_H & \mathcal{D}_H < 0 \\ 0 & \mathcal{D}_H \geq 0 \end{cases} \tag{38}
$$

where α_1 and α_2 are the artificial viscosity parameters, Δx is the element characteristic length. Therefore, the internal energy rate and the Cauchy stress is modified as

$$\dot{e} = \boldsymbol{\sigma} : \boldsymbol{\mathcal{D}} - 3(p+q)\mathcal{D}_H \quad (39)$$

$$\boldsymbol{\sigma} = \boldsymbol{\sigma}_D - (p+q)\boldsymbol{I} \quad (40)$$

4. TIME INTEGRATION

The implementation procedures for updated largrangian formulation of nonlinear dynamic system with frictional contact boundary is described in the following.

Time Integration 1
Preparing for start: set $n = 0$, if the element time step is greater than the critical time step of central difference method, set $\bar{\xi} = 0.58383879542$, otherwise set $\bar{\xi} = 0$, and let matrix $\mathbf{Q}$ is updated for every j step; Decompose the mass matrix $\mathbf{M}$ by $\mathbf{M} = \mathbf{L}^T\mathbf{L}$, and let $\mathbf{q} = \mathbf{L}\mathbf{u}$.

1^o. If $n = 0$ or n is integer time of the j then do following: set $p = n$ and generate the tangential stiffness matrix $\mathbf{K}_p$, form the matrix $\tilde{\mathbf{K}}_p$, $\tilde{\mathbf{Q}}_p$, $\tilde{\mathbf{C}}$, $\overset{*}{\tilde{\mathbf{M}}}$ as

$$\tilde{\mathbf{K}}_p = \mathbf{L}^{-\top}\mathbf{K}_p\mathbf{L}^{-1} \quad (41)$$

$$\tilde{\mathbf{Q}}_p = \mathbf{I} + \frac{(2\bar{\xi}^*\Delta t)^4}{4!}\tilde{\mathbf{K}}_p^2 \quad (42)$$

$$\tilde{\mathbf{C}} = \mathbf{L}^{-T}\mathbf{C}\mathbf{L}^{-1} \quad (43)$$

$$\overset{*}{\tilde{\mathbf{M}}} = \mathbf{I} + \frac{1}{2}\Delta t\tilde{\mathbf{C}} \quad (44)$$

Employing Cholesky decomposition for the matrix $\tilde{\mathbf{Q}}_p$, $\overset{*}{\tilde{\mathbf{M}}}$ as

$$\tilde{\mathbf{Q}}_p = \tilde{\mathcal{L}}^\top\tilde{\mathcal{D}}\tilde{\mathcal{L}} \quad (45)$$

$$\overset{*}{\tilde{\mathbf{M}}} = \tilde{\mathcal{L}}_m^\top\tilde{\mathcal{D}}_m\tilde{\mathcal{L}}_m \quad (46)$$

2^o. If $n = 0$ find $\Delta\mathbf{q}_{n+1}$ by

$$\tilde{\mathcal{L}}^\top\tilde{\mathcal{D}}\tilde{\mathcal{L}}\Delta\mathbf{q}_{n+1} = \Delta t\dot{\mathbf{q}}_n + \frac{1}{2}\Delta t^2\ddot{\mathbf{q}}_n \quad (47)$$

3^o Calculate resultant of stresses within structure $\mathbf{r}_{n+1}$ and the vector $\tilde{\mathbf{r}}_{n+1}$

$$\Delta\mathbf{u}_{n+1} = \mathbf{L}^{-\top}(\Delta\mathbf{q}_{n+1}) \quad (48)$$

$$\mathbf{r}_{n+1} = \mathbf{r}(\sigma_n + \Delta\sigma(\Delta\mathbf{u}_{n+1})) \quad (49)$$

$$\tilde{\mathbf{r}}_{n+1} = \mathbf{L}^{-\top}\mathbf{r}_{n+1} \quad (50)$$

4^o Using return map method to get $\mathbf{s}_T^{n+1}$:

$$\mathbf{s}_T^{n+1} = \mathbf{s}_T^n - \frac{1}{\epsilon}(\Delta\mathbf{g}_T + \mathbf{A}\Delta\lambda_T) \quad (51)$$

5^o. Find ϕ, $\Delta\mathbf{q}_{n+2}$, $\dot{\mathbf{q}}_{n+1}$ and $\ddot{\mathbf{q}}_{n+1}$ by using the linear complementary bi-projection (LCBP) method to solve complementary equation:

$$\lambda(\phi) = \mathbf{N}^\top\tilde{\mathbf{G}}(\tilde{\mathbf{x}}_{n+1} + \Delta\mathbf{q}_{n+2}(\phi)) \geq 0 \quad (52)$$

$$\phi \geq 0 \quad (53)$$

$$\lambda^T(\phi)\phi = 0 \quad (54)$$

6^o. $n := n + 1$ goto 2^o.

Remark 0.1

1. *The algorithm is L-stable and second order accuracy for nonlinear dynamic system with frictional contact boundary when $\bar{\xi}^* > 0.583838795422$.*

2. *The algorithm is the central difference method when $\bar{\xi} = 0$.*

5. Numerical Validation

The numerical example considers experiments conducted by Forrestal and Hanchak with blunt 4340 R_c 38 steel cylinder projectiles impacting circular HY-100 steel plates [Forrestal and Hanchak, 1999]. The material parameter is described in Tabe 1. Quantitatively, the numerical result of the present formulation captures the plug velocity with good agreement as demonstrated in Figure 1. The numerical model effectively captures this plugging failure qualitatively as shown in Figure 2.

Concluding Remarks

In this exposition, we described a continuum damage mechanics based Lagrangian hydrodynamic computational framework for 3D high- and hyper-velocity contact/impact/damage/penetration applications. The contributions of the paper included two aspects: (i) a hydrodynamic constitutive relation including continuum damage mechanics; (ii) a robust time integration algorithm for the coupled equation of state and the internal energy equation. A numerical example were performed to validate the robustness and the accuracy of the proposed framework for the contact/impact/damage/penetration applications.

ACKNOWLEDGMENTS

The authors are very pleased to acknowledge support in part by the Army High Performance Computing Research Center (AHPCRC) under the auspices of the Department of the Army, Army Research Laboratory (ARL) under contract number DAAD19-01-2-0014. The content does not necessarily reflect the position or the policy of the government, and no official

endorsement should be inferred. Other related support in form of computer grants from the Minnesota Supercomputer Institute (MSI), Minneapolis, Minnesota is also gratefully acknowledged.

References

[Bammann et al., 1993] Bammann, D. J., Chiesa, M. L., Horstemeyer, M. F., and Weingarten, L. I. (1993). *Structural Crashworthiness and Failure*, chapter Failure in Ductile Materials Using Finite Element Simulations, pages 1–54. Elsevier, Amsterdam.

[Børvik et al., 2001] Børvik, T., Hopperstad, O. S., Berstad, T., and Langseth, M. (2001). Numerical Simulation of Plugging Failure in Ballistic Penetration. *International Journal of Solids and Structures*, 38:6241–6264.

[Celentano et al., 2004] Celentano, D. J., Tapia, P. E., and Chaboche, J. L. (2004). Experimental and Numerical Characterization of Damage Evolution in Steels. Technical Report 2004-229, ONERA: Tire a Part.

[Forrestal and Hanchak, 1999] Forrestal, M. J. and Hanchak, S. J. (1999). Perforation Experiments on HY-100 Steel Plates with 4340 R_c38 and Maraging T-250 Steel Rod Projectiles. *International Journal of Impact Engineering*, 22:923–933.

[Johnson and Cook, 1985] Johnson, G. R. and Cook, W. H. (1985). Fracture Characteristic of Three Metals Subjected to Various Strains, Strain Rates, Temperatures and Pressures. *Engineering Fracture Mechanics*, 21:31–48.

[Krajcinovic, 2000] Krajcinovic, D. (2000). Damage Mechanics: Accomplishments, Trends and Needs. *International Journal of Solids and Structures*, 37:267–277.

[Lemaitre, 1985a] Lemaitre, J. (1985a). A Continuous Damage Mechanics Model for Ductile Fracture. *Journal of Engineering Materials and Technology*, 107:83–89.

[Lemaitre, 1985b] Lemaitre, J. (1985b). Coupled Elasto Plasticity and Damage Constitutive Equations. *Computer Methods in Applied Mechanics and Engineering*, 51:31–49.

[Lemaitre, 1996] Lemaitre, J. (1996). *A Course on Damage Mechanics*. Springer-Verlag, New York.

[Schraml et al., 2002] Schraml, S. J., Kimsey, K. D., and Clarke, J. A. (2002). High-Performance Computing Applications for Survivability-Lethality Technologies. *Computing in Science and Engineering*, 4:16–21.

[Sha et al., 1996] Sha, D., Tamma, K. K., and Li, M. (1996). Robust Explicit Computational Developments and Solution Strategies for Impact Problems Involving Friction. *International Journal for Numerical Methods in Engineering*, 39:721–739.

[von Neumann and Richtmyer, 1950] von Neumann, J. and Richtmyer, R. D. (1950). A Method for the Numerical Calculation of Hydrodynamic Shocks. *Journal of Applied Physics*, 21:232–237.

[Walsh and Christian, 1955] Walsh, J. M. and Christian, R. H. (1955). Equation of State of Metals from Shock Wave Measurements. *Physical Review*, 97:1544–1556.

[Walsh et al., 1957] Walsh, J. M., Rice, M. H., McQueen, R. G., and Yarger, F. L. (1957). Shock-Wave Compressions of Twenty-Seven Metals. Equation of State of Metals. *Physical Review*, 108:196–216.

[Zhou and Tamma, 2004] Zhou, X. and Tamma, K. K. (2004). Design, Analysis, and Synthesis of Generalized Single Step Single Solve and Optimal Algorithms for Structural Dynamics. *International Journal for Numerical Methods in Engineering*, 59:597–668.

[Zhou et al., 2005] Zhou, X., Tamma, K. K., and Sha, D. (2005). Design Spaces, Measures and Metrics for Evaluating Quality of Time Operators and Consequences Leading to Improved Algorithms By Design - Illustration to Structural Dynamics. *International Journal for Numerical Methods in Engineering*, 64:1841–1870.

[Zukas, 2004] Zukas, J. A. (2004). *Introduction to Hydrocodes*. Studies in Applied Mechanics. Elsevier, P. O Box 211, 1000 AE Amsterdam, The Netherlands.

	HY-100 Steel	4340 R_c 38 steel
Material Properties		
Shear Modulus [GPa]	77.5	77.5
Density [kg/m^3]	7801	7822
JC Strength		
A [MPa]	758.3	600
B [MPa]	402.3	509.5
C	0.011	0.014
T_0 [K]	290	290
T_m [K]	1817	1793
n	0.26	0.26
m	1.13	1.03
C_p [J/kg K]	477	477
JC Fracture		
D_1	-0.61	-0.8
D_2	2.07	2.1
D_3	-0.5	-0.5
D_4	0.01	0.002
D_5	0	0.61
Spall strength [GPa]	5.723	5.723
Fracture strain	0.035	0.035
Damage		
φ_c	0.99	0.99
$\varepsilon_D/\varepsilon_F$	0.6	0.6
EOS		
K_1 [GPa]	164	164
K_2 [GPa]	294	294
K_3 [GPa]	500	500
Γ	1.16	1.16

Table 1: Material constants for HY-100 Steel and 4340 R_c 38 steel

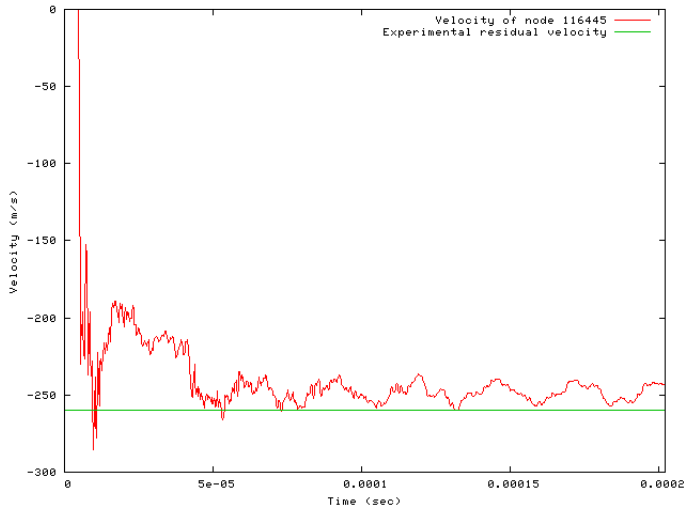

Figure 1: Velocity of plug node 116445 for an impact velocity of 246 m/s. The nodal velocity oscillates close to the experimental value of 260 m/s.

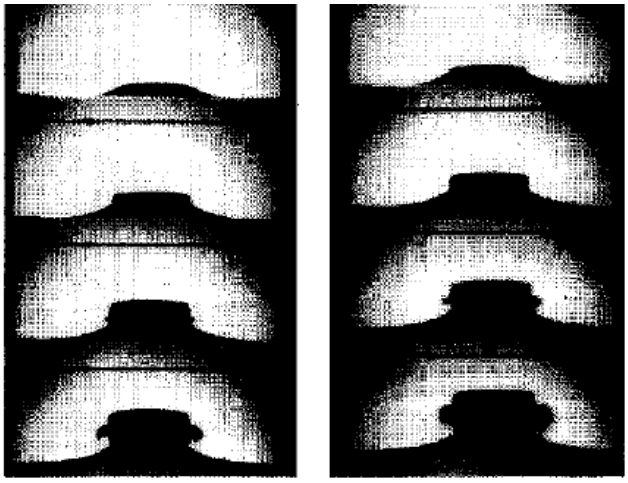

(a) Forrestal-Hanchak experimental results at 10 μs intervals starting at 25 μs for an impact velocity of 246 m/s [Forrestal and Hanchak, 1999]

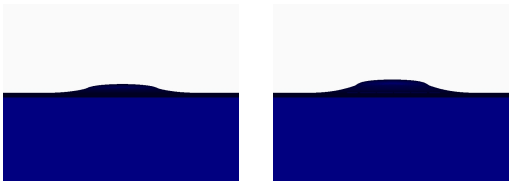

(b) t=25 μs

(c) t=35 μs

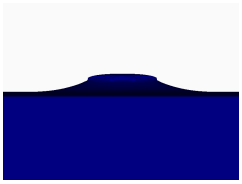

(d) t=45 μs

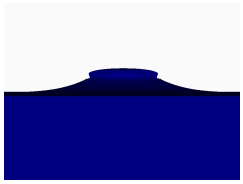

(e) t=55 μs

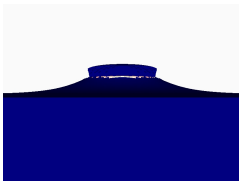

(f) t=65 μs

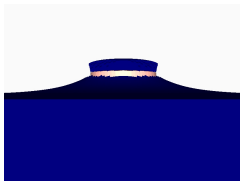

(g) t=75 μs

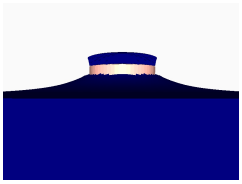

(h) t=85 μs

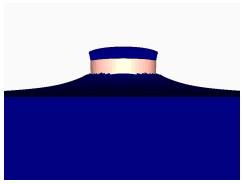

(i) t=95 μs

Figure 2: Comparison of experimental and numerical simulation results showing the plugging failure and dynamic deformation of the HY-100 steel plate for an impact velocity of 246 m/s